Micromachining of mesoporous oxide films for microelectromechanical system structures

Jong-Ah Paik
Department of Materials Science and Engineering, University of California,
Los Angeles, California 90095

Shih-Kang Fan and Chang-Jin Kim
Department of Mechanical and Aerospace Engineering, University of California,
Los Angeles, California 90095

Ming C. Wu
Department of Electrical Engineering, University of California, Los Angeles, California 90095

Bruce Dunn[a]
Department of Materials Science and Engineering, University of California,
Los Angeles, California 90095

The high porosity and uniform pore size of mesoporous oxide films offer unique opportunities for microelectromechanical system (MEMS) devices that require low density and low thermal conductivity. This paper provides the first report in which mesoporous films were adapted for MEMS applications. Mesoporous SiO_2 and Al_2O_3 films were prepared by spin coating using block copolymers as the structure-directing agents. The resulting films were over 50% porous with uniform pores of 8-nm average diameter and an extremely smooth surface. The photopatterning and etching characteristics of the mesoporous films were investigated and processing protocols were established which enabled the films to serve as the sacrificial layer or the structure layer in MEMS devices. The unique mesoporous morphology leads to novel behavior including extremely high etching rates and the ability to etch underlying layers. Surface micromachining methods were used to fabricate three basic MEMS structures, microbridges, cantilevers, and membranes, from the mesoporous oxides.

I. INTRODUCTION

There has been an active effort in the materials chemistry community in recent years to synthesize mesoporous oxides based on the use of sol-gel chemistry in combination with structure-directing agents such as surfactants, block copolymers, and colloidal suspensions.[1–3] In work to date, powders,[4,5] fibers,[6] and thin films[7,8] of various oxides have been produced with varying pore sizes (2 to 30 nm) and organized structures (i.e., hexagonal, cubic, lamellar).[9] Although the specific mechanism for mesostructure formation is the subject of much discussion, there is the general consensus that interactions between the organic and inorganic phases control the means by which mesoscopic order develops, as oxide oligomers assemble around the regularly arranged organic micelles. The mesoporous morphology is formed upon removal of the organic phase by thermal or chemical treatment. Although much of the research to date has emphasized SiO_2, methods have now been extended to a significant number of other metal oxides.[5] In addition, block copolymers have emerged as a convenient group of structure-directing agents for a wide range of oxides.[5] The potential usefulness of mesostructured materials is beginning to attract interest and a number of applications in such areas as separations, catalysis, sensing, optics, and electronics have been discussed.[10–12]

This paper reports the first microelectromechanical system (MEMS) structures to be based on mesoporous oxides. The rapidly emerging technology and applications for MEMS (microelectromechanical systems) are influencing diverse fields from aeronautics, to wireless communications, to optical systems and chemical/biological sensing.[13] Mesoporous oxides are certain to have a role in this technology because of their unique microstructure. For example, mesoporous films can reduce the weight of micromirrors (thereby increasing frequency response), provide thermal insulation to greatly reduce thermal loss of small devices, and serve as a vital component in MEMS device packaging. The fact that a

---

[a] Address all correspondence to this author.

significant number of metal oxides can be prepared as mesoporous materials suggests numerous opportunities for these materials in MEMS systems.

A key factor in incorporating mesostructured materials into MEMS applications is the need to have mesoporous oxides become compatible with micromachining technologies. For example, the photopatterning and etching methods to be used with mesoporous oxides must be similar if not identical to those protocols that have become the basis for MEMS technology. Therefore, the mesoporous materials must be incorporated as films and not powders. The films should be deposited by spin-coating methods, achieve excellent uniformity and smoothness, and have controllable thickness in the 1–2-μm range. While the fabrication of mesoporous films has been reported, including that of spin coating,[14] most of the studies have emphasized the interrelationship between synthesis conditions and the resulting mesostructure with relatively little emphasis on the physical properties and integrity of the film.

The results reported in this work clearly demonstrate that mesoporous oxides are fully compatible with micromachining technologies. The first part of this paper concerns the preparation of selected mesoporous oxides and characterization of their physical and chemical properties. Our results establish that spin coating is a viable method for producing high-quality mesoporous films. The second part of the paper describes our work on the surface micromachining of mesoporous silica and alumina films and demonstrates the fabrication of microbridges, membranes, and cantilevers. It is evident from this work that mesoporous oxide films can be well integrated into MEMS structures.

II. EXPERIMENTAL

A. Film preparation

Mesoporous films of silica and alumina (nominally SiO_2 and Al_2O_3) were prepared by modifying sol-gel methods to incorporate the block copolymer template. Prior research on mesoporous SiO_2 films[7] and sol-gel derived aluminum oxide[15] provided appropriate guidance so that the same general processing approach was followed for each of the oxide films.

The coating solution was prepared in two steps. The first step involved the synthesis of a stable precursor sol. Tetraethyl orthosilicate (Aldrich, Milwaukee, WI) and aluminum *sec*-butoxide (Aldrich) were the precursor alkoxides used for silica and alumina, respectively. A stock solution was prepared from the appropriate alkoxide, ethanol (Fisher Scientific), and HCl (Fisher Scientific, Pittsburgh, PA), in which the alkoxide was only partially hydrolyzed. Excess water and acid were added to the stock solution to produce the coating solution; the molar ratio of water:alkoxide was greater than 10:1 in the coating solution. The composition relationships between the stock solutions and the coating solutions are shown in Table I. There was some difficulty in making clear and stable solutions with the alumina precursor because the condensation reactions proceeded much more rapidly as compared to SiO_2. Therefore, a relatively large amount of acid was added to the stock solution to prevent condensation and to stabilize the coating solution. In the second step, a structure-directing agent was dissolved into the coating solution. The structure-directing agent was a commercially available, amphiphilic, block copolymer which is known to form ordered mesostructures.[16] Specifically, triblock copolymers of the type poly(ethylene oxide)-*block*-poly(propylene oxide)-*block*-poly(ethylene oxide) (PEO–PPO–PEO) were found to be most successful (Pluronic F127 from BASF; $EO_{106}PO_{70}EO_{106}$). The porosity of the final mesoporous film can be tailored by changing the amount of surfactant added to the coating solution, and thus, varying amounts of block copolymer were investigated. For the mesoporous materials described in this paper, approximately 10 wt% block copolymer was added. After homogenous solutions were obtained, films were prepared by spin coating onto silicon substrates. Typical film deposition conditions were 2500 rpm for 60 s. The samples were aged/dried at 100 °C for 24 h and then heated slowly to 400 (silica) or 500 °C (alumina) to burn out the surfactants

TABLE I. Composition of silica and alumina precursor solutions.

	Silica				
Molar ratios	$Si(OC_2H_5)_4$	Ethanol	H_2O	HCl	Pluronic F127 $(EO_{106}PO_{70}EO_{106})$
Molar ratios for stock solution	1	3.8	1	5.1×10^{-5}	$\cdots$
Molar ratios for coating solution	1	15.3	12.3	1.15×10^{-2}	1.44×10^{-2}
	Alumina				
Molar ratios	$Al(OC_3H_7)_3$	Ethanol	H_2O	HCl	Pluronic F127 $(EO_{106}PO_{70}EO_{106})$
Molar ratios for stock solution	1	21	0.55	3.1×10^{-2}	$\cdots$
Molar ratios for coating solution	1	21	17.2	1.82	1.5×10^{-2}

and stabilize the structure and chemistry of the film. The films were kept at the higher temperatures for 2 h and then cooled slowly to room temperature. After burning-out the copolymer, the resulting thickness for a single layer of mesoporous silica and alumina was 500 and 300 nm, respectively. Film thickness was measured by profilometry (Tencor Alpha-Step 200). To achieve a film thickness of 1 to 2 μm for MEMS applications, multilayer coatings were prepared by repeating the above process. Moreover, by changing the coating solution, it was possible to deposit one mesoporous oxide film on top of another (e.g., silica on alumina).

B. Film characterization

The chemical changes which occurred upon heating the mesostructured films were characterized by Fourier transform infrared (FTIR) measurements (MIDAC M2000, Irving, CA) and thermogravimetric analysis (TGA; TA instruments Hi-Res TGA 2950, New Castle, DE). In these experiments, we were generally interested in two features: (i) determining the chemical changes that occurred during heat treatment; (ii) establishing the temperature range over which the copolymer component volatilized from the film. For FTIR measurements, the films were deposited by spin coating onto an IR-transparent substrate (KBr or NaCl). The measurements were made at various stages of the synthesis process: the precursor solution; the hydrolyzed stock solution (before dissolving the copolymer); the coating solution after drying at 100 °C (with copolymer still present); the coating solution after volatilizing the copolymer (400 °C for SiO_2, 500 °C for Al_2O_3). The TGA experiments were carried out on silica and alumina films that were dried at 100 °C for 24 h and then delaminated from the silicon wafer substrate.

The morphology of the final mesoporous films (i.e., after surfactant removal) was characterized using transmission electron microscopy (TEM) and ellipsometry. For the plan-view TEM samples, the mesoporous oxide films were delaminated from the silicon wafer and then placed on a standard copper grid. For cross-section TEM, the sample was placed in a grid which has a hole that matches the thickness of the silicon wafer and then prepared using standard hand grinding, dimpling, and ion-milling steps. The TEM used was a JEOL 2000FX (Tokyo, Japan) operating at 200 kV. Ellipsometry was used to determine the porosity of the final film by measuring the refractive index. On the basis of the Lorentz–Lorenz model,[17] porosity can be calculated as follows:

$$1 - \frac{P}{100} = \left(\frac{n^2 - 1}{n_0{}^2 - 1}\right)\left(\frac{n_0{}^2 + 2}{n^2 + 2}\right) \tag{1}$$

where P is the volume porosity, n_0 is the refractive index of the dense material, and n is the refractive index of the porous material. The refractive index was determined at a wavelength of 632 nm using an ellipsometer (Gaertner L116B, Skokie, IL). It is well known that the refractive index of a porous material is strongly influenced by adsorbed water, a feature which is exploited in moisture sensors.[18] To overcome the difficulties with water adsorption and obtain accurate values of the refractive index, a substrate heater was integrated in the apparatus to heat the samples during the actual ellipsometry measurement. Measurements were made at approximately 150 °C. This temperature removes over 95% of the moisture and has a negligible effect on the refractive index value since dn/dT of SiO_2 is approximately 10^{-5} K^{-1}.[19]

The morphology of mesoporous powders was also determined to serve as a comparison to the results with films. An advantage in using powders is that larger sample sizes are available enabling gas adsorption analysis to be used. Powders were prepared using the same coating solutions, which were cast in glass dishes and heated to 70 °C for 24 h for gelation. Thereafter, the samples were subjected to the same heat treatments as those of the silica and alumina films. The porosity and pore size distribution of the powders were determined using gas adsorption measurements (Micromeritics ASAP 2010, Norcross, GA) with BJH (Barrett, Joyner, Halenda) analysis of the data.

An important requirement for the application of mesoporous oxide films in MEMS devices is that the film be extremely smooth and, in the case of micromirrors,[20] serve as a substrate for reflective coatings. Surface roughness values for the different mesoporous films were determined by interferometry (Wyko RTS 500), (Veeco, Tucson, AZ) imaged over an area of approximately 100 × 100 μm. For the metallization experiments, gold was sputtered (Anatech Ltd. Hummer VI-A sputtering system, Springfield, VA) directly onto the mesoporous oxide films. Reflectivity from 2.5 to 10 μm was determined using the FTIR in the reflection mode and sheet resistivity of the deposited gold layer was measured by a 4-point probe (Prometrix Omnimap RS 35), (KLA Tencor, San Jose, CA).

C. Micromachining of mesoporous films

A vital consideration for surface micromachining processes is to have high etch selectivity. Mesoporous silica and alumina films (1-μm thick) were exposed to wet and dry etchants commonly used in surface micromachining,[27,29] and the qualitative response of the film was recorded. The various etching characteristics were then utilized in subsequent patterning operations.

Lithography of mesoporous films poses new challenges since the photoresist fills the continuous pore network. Because photoresist in the mesopores may not be adequately UV irradiated during exposure, positive photoresist remains in the mesopores even after development and can be deposited as debris when the mesoporous film
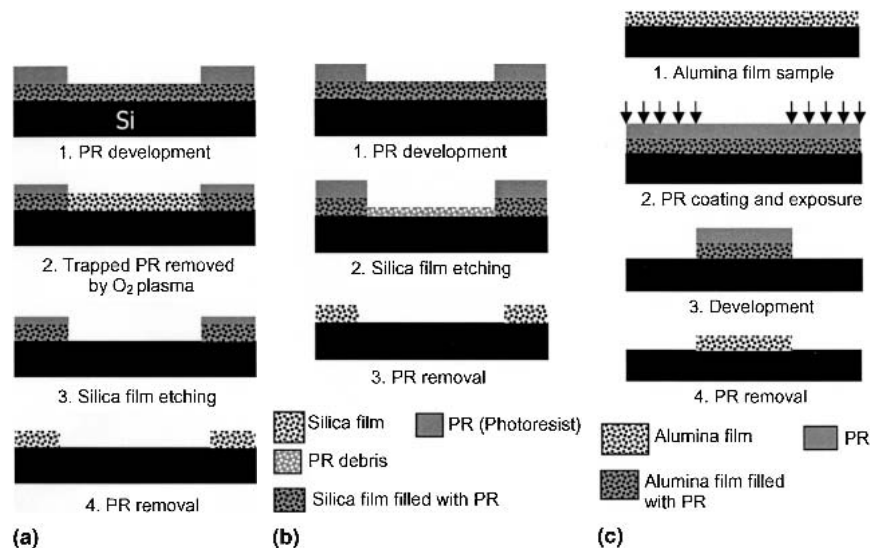
FIG. 1. Patterning of mesoporous oxide films: (a) silica film, trapped photoresist removed before etching; (b) silica film, trapped photoresist removed after etching; (c) alumina film.

is selectively removed. For the patterning of mesoporous SiO_2 films (0.5–2.0-μm thick), we developed two different lithography processes that successfully removed any trapped photoresist (PR). These processes are shown in Figs. 1(a) and 1(b). One approach involves the use of an O_2 plasma before the mesoporous SiO_2 is patterned. A second approach is to use photoresist stripper (acetone or piranha) to remove the photoresist debris after the mesoporous film is etched away.

The lithography process for mesoporous alumina is quite different as shown in Fig. 1(c). Since the mesoporous alumina is slightly soluble in some developers (e.g., AZ 400K developer from Clariant; aqueous solution of potassium borate) (Muttenz, Switzerland), the film can be patterned during the photoresist development step. Thus, a subsequent step of etching the oxide film is not necessary. For developers that do not etch the mesoporous alumina (e.g., AZ developer from Clariant; aqueous solution of trisodium phosphate with silicic acid), it is possible to pattern only the photoresist. This is useful, for example, when a lift-off process is required to pattern metal on top of the mesoporous alumina film. In this case, the lithography process flow is identical to that of the SiO_2 films [Figs. 1(a) and 1(b)] and photoresist trapped in the mesoporous alumina film can be removed either before or after patterning. The choice of developer properties allows considerable flexibility in the lithography process for mesoporous alumina.

III. RESULTS AND DISCUSSION

A. Processing and characterization of mesoporous films

The TGA curves for the silica and alumina films (Fig. 2) indicate that a substantial portion of the copolymer is pyrolyzed at 200 °C but that the copolymer is not
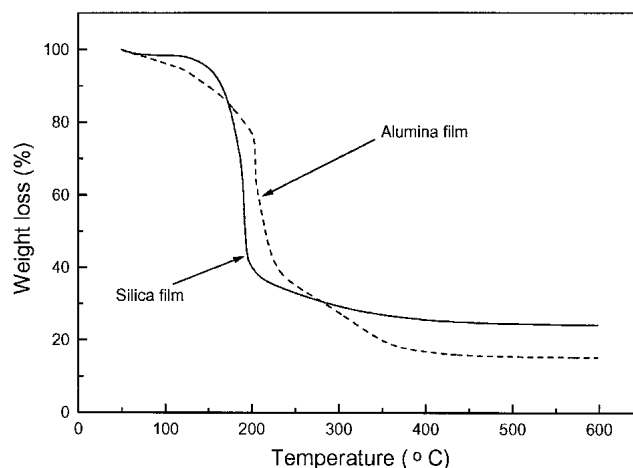

FIG. 2. Thermogravimetric analysis curves for silica and alumina films containing block copolymer. The films were heated in air at a rate of 5 °C/min.

completely removed until 400 °C. The FTIR spectra shown in Fig. 3 display the corresponding chemical changes which occur during heating. For the SiO_2 films shown in Fig. 3(a), the Si–O vibrations at 1072 cm^{-1} (Si–O–Si asymmetric stretching mode) and 800 cm^{-1} (Si–O–Si symmetric stretching mode)[21] were observed in films made from the stock solution and throughout the various film processing stages. Peaks related to the copolymer at 2916 cm^{-1} (C–H stretching mode) and 1450 cm^{-1} (C–H bending mode)[22] appeared in the films dried at 100 °C. These peaks disappeared after the 400 °C heat treatment indicating that this is a good processing temperature for the SiO_2 mesoporous film because the copolymer is fully removed and the SiO_2 network undergoes no further chemical changes. FTIR was also used to characterize chemical changes occurring in the alumina films.

(a) Wave number (cm⁻¹)
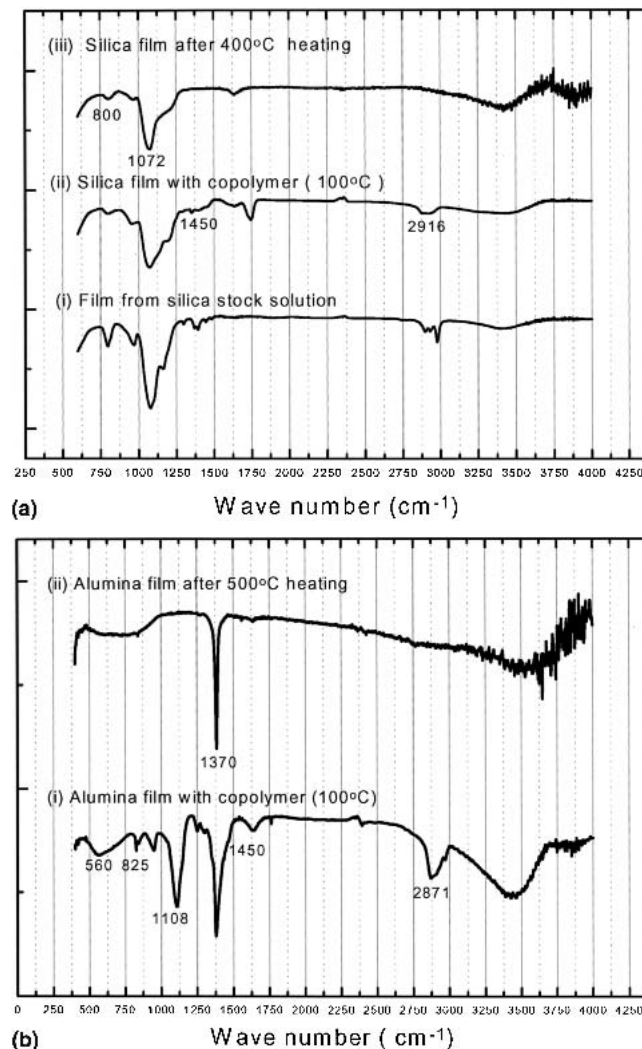

(b) Wave number (cm⁻¹)

FIG. 3. Infrared absorption spectra for silica and alumina films at different stages of processing, (a) FTIR of silica films: (i) silica film from stock solution; (ii) silica film with copolymer and heated to 100 °C; (iii) final silica film after heating at 400 °C. The peaks at 800 and 1072 cm⁻¹ are from Si–O vibrations (symmetric and asymmetric stretching mode, respectively). The peaks at 1450 and 2916 cm⁻¹ are C–H vibrations (bending and stretching mode, respectively) from the addition of the copolymer. (b) FTIR of alumina films: (i) alumina film with copolymer and heated to 100 °C; (ii) final alumina film after heating at 500 °C. The peaks at 560 and 825 cm⁻¹ are from Al–O vibrations (stretching with octahedral and tetrahedral coordination, respectively). The peaks at 1450 and 2871 cm⁻¹ are C–H vibrations (bending and stretching mode, respectively) from the addition of the copolymer. The peak at 1108 cm⁻¹ is a C–O vibration (stretching mode) from the addition of the copolymer. The peak at 1370 cm⁻¹ indicates that some of the precursor is retained in the film.

The Al–O bonds at 825 cm⁻¹ (Al–O stretch with tetrahedral coordination) and 560 cm⁻¹ (Al–O stretch with octahedral coordination)[23] were apparent in the stock solution and in the final films, while the copolymer peaks (2871 cm⁻¹ for C–H stretching mode, 1108 cm⁻¹ for C–O bond stretching mode, and 1450 cm⁻¹ for C–H bending mode)[22] disappeared upon heating to 500 °C. One

interesting feature is that a peak corresponding to Al–O–R at 1370 cm⁻¹, which is part of the aluminum precursor,[24] did not convert to Al–O bonds. This bond is present even after heating to 500 °C indicating that it is thermally stable. The Al–O–R bond may be responsible for the observed etching of the oxide film in HF and in base, since α–Al_2O_3 films are normally insoluble in these solvents.

The TEM images (Fig. 4) clearly show that the mesoporous oxide films are very porous and possess a uniform pore diameter. More detailed analysis indicates that the average pore diameter is on the order of 8 nm. There is virtually no difference between the plan-view and cross-section TEM images indicating that there is no particular orientation to the pores. The cross-section image establishes that the porosity is continuous through the film and, in view of the high level of porosity, provides a reasonable basis for concluding that the porosity is interconnected. The pores are not ordered; however, this may be due to the specific solution composition investigated. Recent results with alkylammonium surfactants suggest that ordering in spin-coated films is determined by the composition of the deposited solution.[14]

The porosity of the films, as determined by refractive index measurements and Eq. (1), is in excess of 50%. This calculation requires a value for the corresponding dense oxide [i.e., n_0 in Eq. (1)]. A value of 1.46 was chosen for SiO_2 based on separate measurements of LPCVD (low pressure chemical vapor deposition) grown SiO_2. The reference refractive index for the aluminum oxide was chosen to be 1.665[25] because these films, even after heating to 500 °C, are amorphous. As expected, the refractive index decreases as the film is heated to 150 °C because of moisture desorption. Table II compares the porosity, pore size, and pore size distribution for both thin films and powders of mesoporous silica and alumina. The higher porosity for the powders can be attributed to the very different drying process associated with powder synthesis as compared to spin-coated films.

The heat-treated mesoporous films are extremely smooth (Table II). The 5-nm value is quite significant when one considers that these are highly porous films with an average pore diameter of approximately 8 nm. There is no difficulty in using the mesoporous films as substrates for metal deposition. The IR reflectivity (2.5 to 10 μm) from 100-nm gold films sputtered onto mesoporous SiO_2 films was identical to that of a reference sample of gold sputter deposited on a bare silicon wafer (Fig. 5). The electrical resistivity values for 100-nm gold layers e-beam evaporated on either mesoporous SiO_2 or SiO_2 prepared by low-pressure chemical vapor disposition were virtually identical, approximately 3×10^{-6} Ω cm. This value compares quite well with that reported in the literature.[26] These experiments establish that the metallized layers deposited on mesoporous oxide films are continuous, conductive and highly reflective.
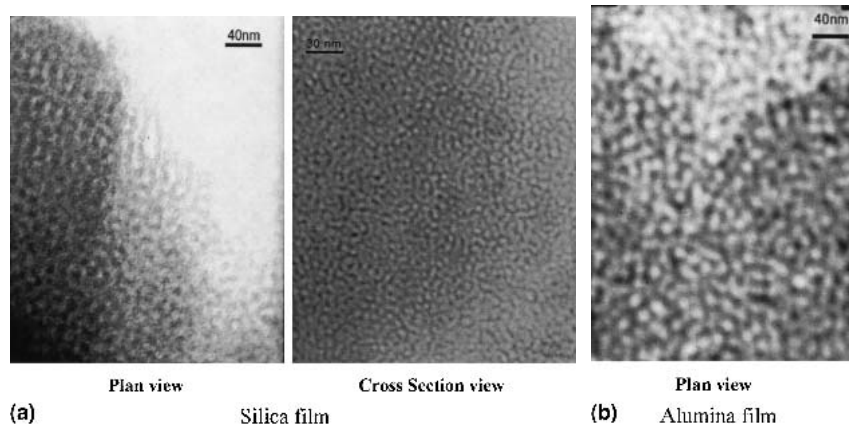
FIG. 4. TEM images for silica and alumina films.

TABLE II. Comparison between film properties and powder properties.

	Film properties			Powder properties		
	Ave. pore diameter (nm)	Porosity (%)	Roughness (nm)	Ave. pore diameter (nm)	Porosity (%)	Pore volume (cm^3/g)
Silica	~8	55	4.88	7 ± 3	72	1.16
Alumina	~8	64	4.87	6 ± 2	70	0.80
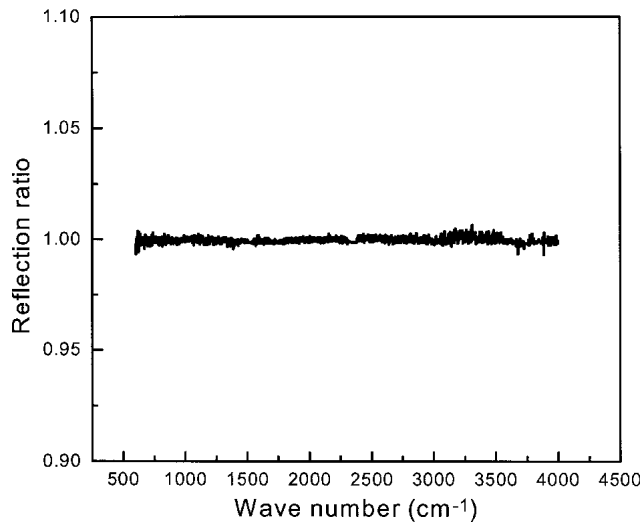
FIG. 5. Infrared reflectivity for gold sputter deposited on mesoporous silica film. The data are referenced to the reflection of gold sputtered directly on silicon. The resulting ratio is equal to one over most of the spectrum indicating that the reflectivity for gold is unaffected by having the mesoporous silica serve as the substrate.

B. Micromachining of mesoporous films

Surface micromachining methods are well-known processes but have not been used with deposited porous materials.[27] The critical issue we address in these studies is whether these micromachining processes can be extended to deposited mesoporous oxide films. The first item to be considered was the response of mesoporous silica and alumina films toward various etchants that are commonly used in surface micromachining. The high surface area and thin solid phase ensure that these porous films will etch much faster than nonporous films. A high etch selectivity and rate are advantageous for surface micromachining processes because it facilitates the release of large area structures. For example, the etch rate for mesoporous SiO_2 in buffered oxide etchant (BOE; see Table III) is over 30 times faster than that of PSG (phosphosilicate glass), which is commonly used as a sacrificial layer in the MUMPs (multiuser MEMS processes) process.[28] Thus, the etch selectivity will increase substantially by utilizing mesoporous SiO_2 rather than PSG as the sacrificial layer.

The etching selectivity also enables mesoporous oxide films to be both the sacrificial layer and the structure layer. We have produced mesoporous SiO_2 structures by using mesoporous alumina as the sacrificial layer. As shown in Table III, the photoresist developer, AZ 400K, is a highly selective etchant for the mesoporous alumina films. The unhydrolyzed part of the aluminum oxide (Fig. 3) is likely to play a role in making the oxide susceptible to etching in mild base solution.

Dry etching processes are particularly interesting because it is possible to use the mesoporous oxide as a structural material with a nonporous sacrificial layer. We have investigated this approach in considerable detail, and as described below, have produced free-standing mesoporous alumina structures by using silicon as a sacrificial layer. XeF_2 is the best candidate for this process. In addition to a high etch selectivity between silicon and mesoporous alumina, XeF_2 can etch silicon isotropically

and undercut the silicon wafer to facilitate release of the structure. Reactive ion etching (RIE) of silicon has also proven to be an effective means for releasing mesoporous alumina structures, even though it is not as isotropic.

One of the unique features of mesoporous oxides is that etchants penetrate the interconnected porous film and react with the underlying layer. To produce anchored structures, modified concepts for sacrificial etching need

TABLE III. Etching responses for silica and alumina mesoporous films

Etchants	1-μm alumina film	1-μm silica film
HF	<5 s	<1 s
BOE[a]	1 min	5 s
Piranha[b]	Etched	No apparent etching
AZ 400K[c]	~2 min	No apparent etching (>10 min)
XeF$_2$[d]	No apparent etching (>120 pulses)	<5 pulses
RIE[e]	No apparent etching (>30 min)	~2 min
DRIE (deep reactive ion etching)	No apparent etching (>10 min)	~3 min

[a]40% ammonium fluoride:49% HF = 6:1.
[b]Sulfuric acid:hydrogen peroxide = 5:1.
[c]Deionized water:AZ 400K = 5:1.
[d]Pulse duration of 2 min.
[e]Pressure ratio of reactant gases: CF_4:O_2 = 5:1. Power: 200 W.

to be developed. As shown in Fig. 6, the anchors can be defined either by depositing etch-resistant thin films underneath or on top of the mesoporous layer. Although silicon is shown as the sacrificial layer, it should be appreciated that a discrete layer can be used to control the gap accurately.

We have demonstrated the micromachining of mesoporous oxides and produced bridges, cantilevers, and membranes using surface micromachining approaches.[27] The initial work has focused on mesoporous alumina structures released by XeF$_2$ dry etching of the silicon substrate. An array of microbridges made of 0.8-μm-thick mesoporous alumina is shown in Fig. 7(a). With this process, we have successfully released cantilevers up to 1100 μm long with a gap of approximately 5 μm [Fig. 7(b)]. The relatively flat cantilevers of this length and thickness indicate a very low stress gradient in the film. The mechanical properties of mesoporous oxide films are currently under investigation. The fabrication of mesoporous membranes has also been achieved. The process flow and resulting membranes are shown in Fig. 8. Membranes sized from 100 × 100 μm to 1000 × 1000 μm have been successfully released by XeF$_2$ etching through the mesoporous alumina films.

(a)
1. Alumina coating and patterning
2. Anchor deposition and patterning
3. Sacrificial etching

Silicon
Alumina
Etch-resistant thin film (anchor material)

(b)
1. Anchor deposition and patterning
2. Alumina coating
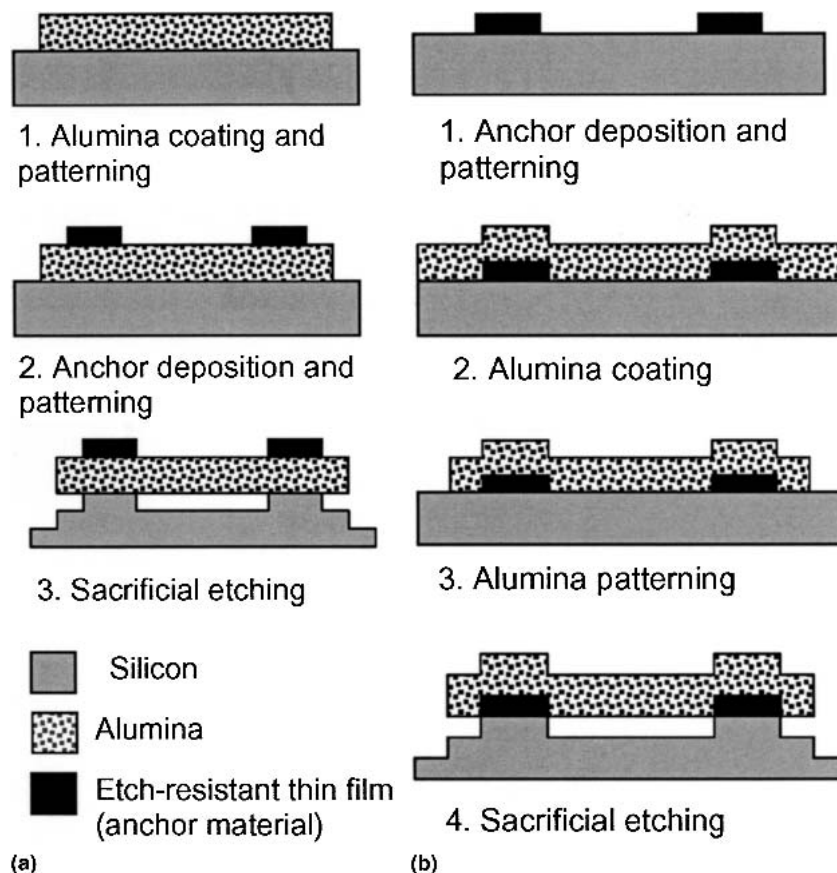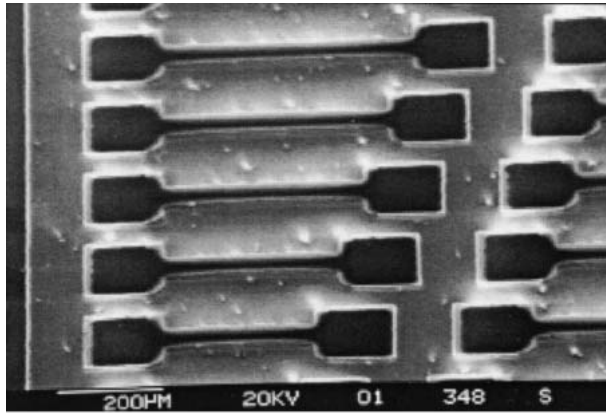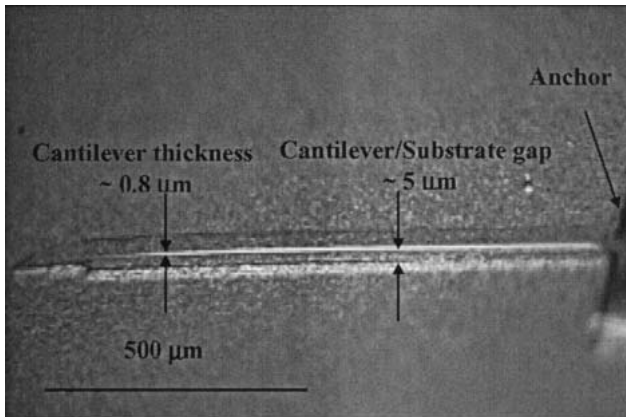3. Alumina patterning
4. Sacrificial etching

FIG. 6. Anchoring schemes for sacrificial etching of mesoporous alumina: (a) anchor deposited onto mesoporous film; (b) mesoporous film deposited over anchor.

(a) Micro bridges

(b) Cantilever

FIG. 7. Mesoporous alumina fabricated into microbridges and cantilevers. The structures were released by XeF_2 dry etching of the silicon substrate.

The micromachining of mesoporous oxides uses the intrinsic porosity as natural etching holes. Removing the sacrificial layer underneath a large mesoporous oxide layer is not a problem; etchants penetrate the exposed surface. This approach contrasts with standard methods based on using nonporous materials where the sacrificial layer must be removed by undercut etching and the process is severely limited by diffusion. Another significant point is that it is possible to use RIE to release mesoporous structures since undercutting from the edge of the structure is not required. Moreover extremely small gaps between the released structure and the substrate can be achieved.

IV. CONCLUSIONS

This paper represents the first report of using mesoporous oxides in MEMS structures. Films are prepared by spin coating, a method rarely used for the deposition of mesoporous oxide films. Synthesis methods based on
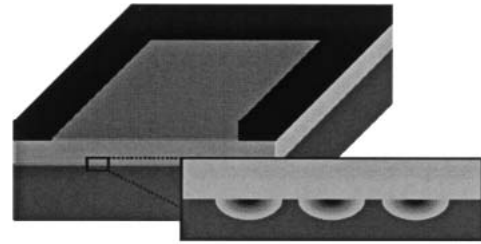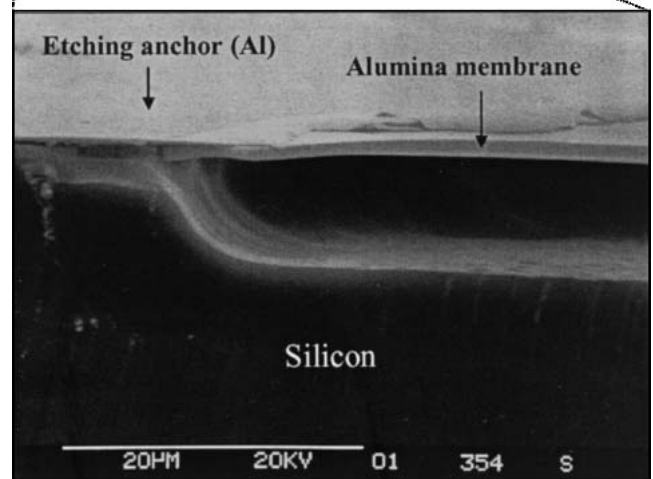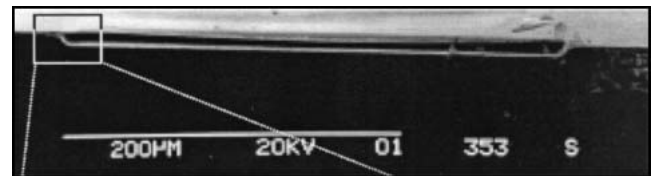

1. Etchant (XeF_2) penetrates through alumina mesoporous film to attack sacrificial layer
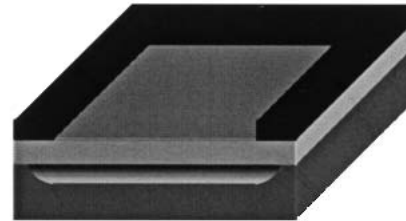
2. Alumina mesoporous membrane obtained

Silicon wafer — Etch-resistant anchor
Alumina mesoporous film

(a)

(b)

FIG. 8. Fabrication of mesoporous membranes of alumina; (a) process flow for membrane fabrication, with the aluminum anchor deposited on top of the mesoporous film and protecting the underlying silicon from the XeF_2 etchant; (b) cross section of a mesoporous alumina membrane.

the use of block copolymers as structure-directing agents lead to highly porous thin films with very small pore diameters (<10 nm) and uniform pore size. The porous morphology has little effect on metallization. Mesoporous silica and alumina films can be processed by standard surface micromachining methods, although some additional steps are necessary, such as the removal of residual photoresist. There are also beneficial effects from the unique mesoporous morphology. The thin solid network leads to an extremely high etch rate while the interconnected porous network allows etchants to rapidly penetrate through the film and attack the underlying layer. The latter behavior was used to release mesoporous alumina from a nonporous sacrificial layer, the silicon substrate. Three basic MEMS structures, cantilevers, microbridges, and membranes, were fabricated using this approach, demonstrating the feasibility of integrating mesoporous oxides into this technology. Mesoporous materials are likely to be important for MEMS devices that require low density and low thermal conductivity. However, with the large number of mesoporous oxides available, applications in the areas of catalysis, fluidics, and optics are likely to develop. Our current efforts are directed at integrating mesoporous oxides in micromirrors.

ACKNOWLEDGMENT

REFERENCES

1. N.K. Raman, M.T. Anderson, and C.J. Brinker, Chem. Mater. **8,** 1682 (1996).
2. D. Zhao, P. Yang, Q. Huo, B.F. Chmelka, and G.D. Stucky, Curr. Opin. Solid State Mater. Sci. **3,** 111 (1998).
3. A. Van Blaaderen, R. Ruel, and P. Wiltzius, Nature **385,** 321 (1997).
4. C.T. Kresge, M.E. Leonowicz, W.J. Roth, J.C. Vartuli, and J.S. Beck, Nature **359,** 710 (1992).
5. P. Yang, D. Zhao, D.I. Margolese, B.F. Chmelka, and G.D. Stucky, Chem. Mater. **11,** 2813 (1999).
6. H. Yang, G.A. Ozin, and C.T. Kresge, Adv. Mater. **10,** 883 (1998).
7. D. Zhao, P. Yang, N. Melosh, J. Feng, B.F. Chmelka, and G.D. Stucky, Adv. Mater. **10,** 1380 (1998).
8. Y. Lu, R. Ganguli, E.A. Drewien, M.T. Anderson, C.J. Brinker, W. Gong, Y. Guo, H. Soyez, B. Dunn, M.H. Huang, and J.I. Zink, Nature **389,** 364 (1997).
9. D. Zhao, Q. Huo, J. Feng, B.F. Chmelka, and G.D. Stucky, J. Am. Chem. Soc. **120,** 6042 (1998).
10. P. Yang, T. Deng, D. Zhao, P. Feng, D. Pine, B.F. Chmelka, G.M. Whitesides, and G.D. Stucky, Science **282,** 2244 (1998).
11. P. Yang, G. Wirnsberger, H.C. Huang, S.R. Cordero, M.D. McGehee, B. Scott, T. Deng, G.M. Whitesides, B.F. Chmelka, S.K. Buratto, and G.D. Stucky, Science **287,** 465 (2000).
12. R.C. Hayward, P. Alberius-Henning, B.F. Chmelka, and G.D. Stucky, Microporous Mesoporous Mater. **44–45,** 619 (2001).
13. See the special issue of MRS Bull. April 2001: *Microelectromechanical Systems: Technology and Applications,* guest edited by D. Bishop, A. Heuer and D. Williams, p. 282.
14. (a) S. Besson, T. Gacoin, C. Jacquiod, C. Ricolleau, D. Babonneau, and J-P. Boilot, J. Mater. Chem. **10,** 1331 (2000); (b) S. Besson, C. Ricolleau, T. Gacoin, C. Jacquiod, and J-P. Boilot, J. Phys. Chem. B **104,** 12095 (2000).
15. D.J. Suh and T-J. Park, Chem. Mater. **9,** 1903 (1997).
16. B. Chu and Z. Zhou, in *Nonionic Surfactants: polyoxyalkylene block copolymers,* edited by V.M. Nace (Marcel Dekker, New York, 1996), p. 67.
17. M. Born and E. Wolf, *Principles of Optics* (Pergamon Press, Oxford, U.K., 1986).
18. F. Mitschke, Opt. Lett. **14,** 967 (1989).
19. J. Matsuoka, N. Kitamura, S. Fujinaga, T. Kitaoka, and H. Yamashita, J. Non-Cryst. Solids **135,** 86 (1991).
20. N. Clark, MRS Bull. **26,** 320 (2001).
21. I.H. Joe, A.K. Vasudevan, G. Aruldhas, A.D. Damodaran, and K.G.K. Warrier, J. Solid State Chem. **131,** 181 (1997).
22. C. Guo, H.Z. Liu, and J.Y. Chen, Colloid Polym. Sci. **277,** 376 (1999).
23. A. Bertoluzza, C. Fagnano, M.A. Morelli, V. Gottardi, and M. Guglielmi, J. Non-Cryst. Solids **48,** 117 (1982).
24. N. Ozer, J.P. Cronin, Y.J. Yao, and A.P. Tomsia, Sol. Energy Mater. Sol. Cells **59,** 355 (1999).
25. V.J. Silvestri, C.M. Osburn, and D.W. Ormond, J. Electrochem. Soc. **125,** 902 (1978).
26. T. Yasuyuki and S.M. Tadashi, J. Vac. Sci. Technol., A **16,** 2042 (1998).
27. M.J. Madou, *Fundamentals of Microfabrication* (CRC Press, New York, 1997).
28. K.R. Williams and R.S. Muller, J. Microelectromech. Syst. **5,** 256 (1996).
29. S.D. Senturia, *Microsystem Design* (Kluwer Academic Publishers, Boston, MA, 2000).